Nonlinear Surface Lattice Resonance in Plasmonic Nanoparticle Arrays

Lior Michaeli,[1,2,*] Shay Keren-Zur,[1] Ori Avayu,[1] Haim Suchowski,[2,3] and Tal Ellenbogen[1,3]
[1]Department of Physical Electronics, Faculty of Engineering, Tel-Aviv University, Tel-Aviv 6779801, Israel
[2]Raymond and Beverly Sackler School of Physics & Astronomy, Tel-Aviv University, Tel-Aviv 6779801, Israel
[3]Center for Light-Matter Interaction, Tel-Aviv University, Tel-Aviv 6779801, Israel
(Received 7 February 2017; published 16 June 2017)

We study experimentally second-harmonic generation from arrays of split-ring resonators at oblique incidence and find conditions of more than 30-fold enhancement of the emitted second harmonic with respect to normal incidence. We show that these conditions agree well with a nonlinear Rayleigh-Wood anomaly relation and the existence of a surface lattice resonance at the second harmonic. The existence of a nonlinear surface lattice resonance is theoretically confirmed by extending the coupled dipole approximation to the nonlinear case. We further show that the localized surface plasmon modes that collectively contribute to the surface lattice resonance are inherently dark modes that become highly bright due to the collective interaction.

DOI: 10.1103/PhysRevLett.118.243904

The artificial structural nonlinearity of metallic nanoparticles has been shown recently to enable nonlinear optical conversion with large effective nonlinear coefficients and in a variety of light manipulation schemes [1–10]. The interest in this field was stimulated by Sir John Pendry's prediction of high nonlinearities of structured materials [11]. The ability to obtain controlled nonlinearity by modifying the geometry of nanostructured materials opens the door to new fundamental studies in the realm of nonlinear optics. Several studies have been performed in recent years on trying to unveil the fundamental mechanisms for the measured artificial nonlinearity, mainly focusing on the single plasmonic nanoparticle [1,12,13]. It was shown that the strong quadratic nonlinearity origins from a combination of several effects [12–16], including local symmetry breaking on the interface of the nanostructure, the field enhancement due to excitation of localized surface plasmons resonances (LSPRs), asymmetry of the nanostructure which leads to efficient generation of nonlinear currents in a bright emission mode at the nonlinear output, and good spatial overlap between the localized modes participating in the nonlinear interaction.

It was also shown that the single nanostructure second-harmonic (SH) emission can be substantially modified when placed at an array of similar particles, with dependence on the lattice symmetry, orientation, and spacing [2,3,17]. In the subdiffraction regime, where the lattice spacing is sufficiently small to allow only zero-order forward and backward scattering of the fundamental frequency (FF) and the generated nonlinear beams, the net nonlinear optical response stems predominantly from the single particle nonlinearity, with near-field influenced variations due to the coupling between adjacent nanoparticles. Richer control of the optical response due to lattice structure can be achieved at the photonic regime of the SH, i.e., for lattice spacing that allows higher order diffraction of the SH wavelength [6]. While both regimes were much explored, the boundary in between, where the SH light diffracts on the surface and long range collective interactions play a vital role in the optical response, has received less attention to date.

In the linear case, the condition of diffraction into a surface wave is known as the Rayleigh anomaly (RA) [18]. It was shown that arrays of metallic nanoparticles show sharp spectral features when the RA condition crosses a LSPR condition due to hybridization of the surface and localized resonances, which results in a so-called surface lattice resonance (SLR) [19–21]. In the past decade linear dynamics of SLRs have been explored extensively in lattices made out of different shapes of the constituent metallic nanostructures [19–25], different lattice symmetries [26], and at different frequency ranges from the visible and near infrared [19–27] to the THz frequencies [28,29]. They have also shown a potential in various fields including sensing [30], generation of coherent light sources [31], nonlocal coupling of the magneto-optical response of magnetic nanoparticles [32,33], and for solid-state lighting [34]. The case of nonlinear diffraction from metallic gratings has also been studied extensively [35–37]. However, the effect of SLRs on the nonlinear optical response of nanostructured materials has been studied only in a minute amount of works. In a recent work by Kauranen's group, tenfold enhancement of second-harmonic generation (SHG) was measured due to the existence of SLR at the FF [38]. Yet, the dynamics of the nonlinear response due to nonlinear collective interactions, i.e., SLR at the generated nonlinear mode, has remained unexplored.

In this study we experimentally demonstrate, for the first time to our knowledge, nonlinear SLR (NL-SLR) as a result of nonlinear RA (NL-RA) coupled to a localized mode in rectangular arrays of split-ring resonators (SRRs). We derive a theoretical expression for the NL-SLR condition by extending the coupled dipole approximation to the nonlinear case. The resulting extension for the collective nonlinear quadratic response takes a similar form to Miller's rule.

We also show analogy between our nonlinear results and the famous Wood's anomalies observed in 1902 for linear diffraction from metallic gratings [39]. Specifically, we observe sharp resonant response due to the nonlinear excitation of the surface lattice waves. This results in more than 30-fold enhancement of the SHG with respect to normal incidence, due to the coherent nonlinear interaction between the isolated nanoparticles as the condition of the NL-SLR is satisfied. In addition we observe abrupt change in the collected nonlinear light from both spectral sides of the calculated NL-RA condition. Finally, we show that the NL-SLR and its corresponding linear SLR rise from hybridization of a lattice mode and a dark localized surface plasmon (LSP) mode, in contrast to most of the previous reports of SLRs [19–23,26–28], showing that the plasmonic mode that contributes to the SLR is a bright dipole mode.

To study the optical response associated with SLRs on nanoparticles arrays the coupled dipole approximation (CDA) [40,41] method is often used. This model aims to find the collective optical response through the presentation of effective polarizability of each of the particles in the presence of the array, α_{eff}, which is a function of the single particle polarizability α_s, its radiation pattern, and the array geometry. The polarization at the ith nanoparticle is

$$P_i = \alpha_s E_{\mathrm{loc},i}, \tag{1}$$

where $E_{\mathrm{loc},i}$ is the local electric field at the ith particle location, which is composed of the applied field, E_{app}, and the scattered field from all other dipoles,

$$E_{\mathrm{loc},i} = E_{\mathrm{app}} + \sum_{j\neq i} A_{ij}\alpha_s E_{\mathrm{loc},j}. \tag{2}$$

A_{ij} is the dipole interaction matrix that depends on geometrical parameters and on the wave vector and describes the interaction between the ith and jth dipoles. Considering higher multipole interactions can be done by modifying A_{ij} accordingly. By substituting Eq. (2) into Eq. (1) a set of linear equations can be attained, which can be solved numerically to obtain the polarization at each array site. At the specific case of normal incidence, the above relations can be simplified by assuming that the local electric fields at all array sites are the same, $E_{\mathrm{loc},i} = E_{\mathrm{loc},j} \equiv E_{\mathrm{loc}}$. Then by defining the retarded dipole sum as $S \equiv \sum_{j\neq i} A_{ij}$, the expression for the local field is obtained:

$$E_{\mathrm{loc}} = \frac{E_{\mathrm{app}}}{1 - S\alpha_s}, \tag{3}$$

where S is a complex parameter that has a resonance in the vicinity of the RAs condition. By requiring that the interparticle influence will be taken into account through effective polarizability, i.e., fulfilling the relation $P_i = \alpha_{\mathrm{eff}} E_{\mathrm{app}}$, we get

$$\alpha_{\mathrm{eff}} = \frac{\alpha_s}{1 - S\alpha_s}. \tag{4}$$

From this formula it is possible to obtain insights on the SLR condition. We expect a strong response at the vicinity of the LSPR as a result of the proportionality of the array polarizability to the single particle polarizability. In addition, when the real part of $1/\alpha_s - S$ vanishes we expect resonance due to the lattice effect.

Here, we extend the above linear derivation to the nonlinear case of three-wave mixing (TWM) and introduce an expression for the effective second-order nonlinear polarizability, β_{eff}, which accounts for the array effect. For an array being irradiated with two light beams of frequencies ω_1 and ω_2 the polarization at $\omega_3 = \omega_1 \pm \omega_2$ of the ith nanoparticle can be expressed as

$$P_i(\omega_3) = \frac{1}{2}\beta_s E_{\mathrm{loc},i}(\omega_1) E_{\mathrm{loc},i}(\omega_2) + \alpha_s E_{\mathrm{loc,i}}(\omega_3), \tag{5}$$

where, β_s is the single particle second-order nonlinear polarizability. $E_{\mathrm{loc},i}(\omega_k)$ for $k = 1, 2$ follows the same relation as in Eq. (2) and $E_{\mathrm{loc},i}(\omega_3)$ is composed of the scattered light at ω_3 from all the $j \neq i$ lattice sites,

$$E_{\mathrm{loc},i}(\omega_3) = \sum_{j\neq i} A_{ij}(\omega_3) p_i(\omega_3). \tag{6}$$

Considering again the case of normal incidence and requiring that the array effect will be manifested through the presentation of effective quadratic polarizability, we get

$$\beta_{\mathrm{eff}}(\omega_3;\omega_1,\omega_2) = \frac{\beta_s(\omega_3;\omega_1,\omega_2)}{[1 - S(\omega_1)\alpha_s(\omega_1)][1 - S(\omega_2)\alpha_s(\omega_2)][1 - S(\omega_3)\alpha_s(\omega_3)]}. \tag{7}$$

This result for the nonlinear polarizability β_{eff} takes a similar form to that of the quadratic susceptibility described by the local Miller's rule [42,43], whereas the localized resonances that give rise to the enhanced $\chi^{(2)}$ in Miller's rule are replaced by the linear and nonlinear SLR conditions, $\mathrm{Re}\{S(\omega_k)\alpha_s(\omega_k)\} = 1$ and $\mathrm{Re}\{S(\omega_3)\alpha_s(\omega_3)\} = 1$, respectively. Therefore, this result accounts for a more general case where, in addition to local resonances, there can also be collective lattice resonances. When the lattice spacing affords only diffraction at ω_3 we expect $S(\omega_k) \approx 0$ and enhancement of the nonlinear polarizability will be when the LSPR at ω_3 and the NL-RA, manifested by $\alpha_s(\omega_3)$ and by $S(\omega_3)$, respectively, will get into close proximity.

To find the condition of NL-RA that describes the nonlinear generation of waves traveling at a grazing angle

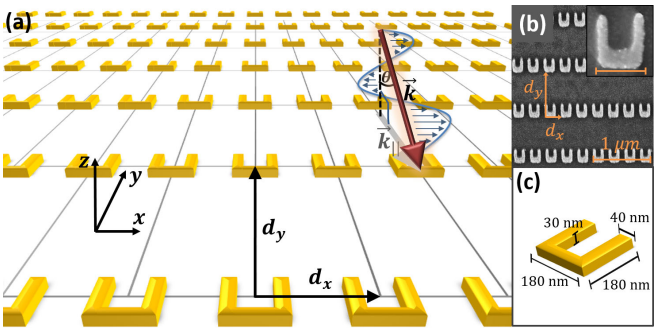

FIG. 1. (a) Illustration of the studied SRRs array, incident angle, and polarization. The incident light wave vector lies in the y-z plane at an angle θ relative to the normal to the surface. (b) Scanning electron microscope image of the fabricated sample. The inset shows a single SRR. (c) Illustration of the physical dimensions of each SRR.

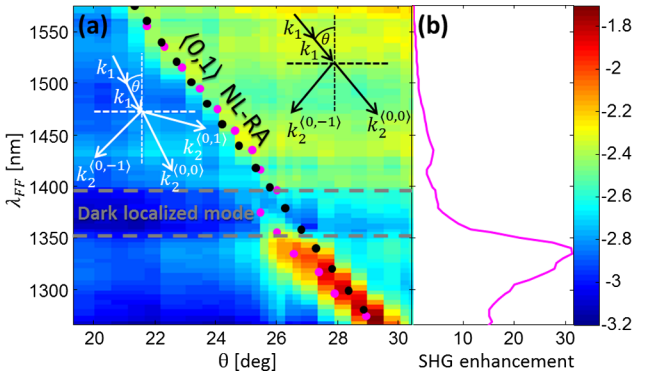

FIG. 2. Second-harmonic emission, NL-RA and NL-SLR. (a) Log scale of the measured zero-order SHG emission vs the FF wavelengths and the incident angle. The black dots indicate the NL-RA of $\langle 0,1\rangle$ order calculated according to Eq. (11), and the magenta dots indicate the strongest measured response at each wavelength. The arrows diagrams demonstrate the existing diffraction modes in both sides of the NL-RA. (b) SHG enhancement along the position of strongest measured emission relative to normal incidence.

to the surface, the linear RA condition can be generalized to the nonlinear case. The linear condition stated in terms of momentum conservation is given by

$$\vec{k}_{\parallel} + \vec{G}_{m_1,m_2} = \vec{k}_s, \tag{8}$$

where $\vec{k}_{\parallel}$ is parallel to the surface component of the incident wave vector $\vec{k} = [2\pi \cdot n(\lambda)/\lambda]\hat{k}$, $n(\lambda)$ is the refractive index, $\vec{G}_{m_1,m_2} = m_1\vec{b}_1 + m_2\vec{b}_2$ is a general reciprocal lattice vector that is a linear combination of the primitive lattice vectors, and $\vec{k}_s = |\vec{k}|\hat{k}_s$ is the surface scattered wave. The vectors $\hat{k}$ and $\hat{k}_S$ are unit vectors specifying the directions of the incident wave vector and the scattered surface wave vector.

Extending the RA momentum conservation requirement to the nonlinear Raman-Nath diffraction regime [44] for TWM gives

$$(\vec{k}_1)_{\parallel} + (\vec{k}_2)_{\parallel} + \vec{G}_{m_1,m_2} = \vec{k}_{3,s}, \tag{9}$$

where k_i ($i = 1, 2,3$) corresponds to the beam at ω_i.

In the particular case of SHG studied here $\omega_1 = \omega_2 = \omega$ and $\omega_3 = 2\omega$. In addition, the incident angle θ varies only in the y-z plane [Fig. 1(a)], and $m_1 = 0$, which sets $\vec{G}_{m_1,m_2} = m_2(2\pi/d_y)\hat{y}$, where d_y is the y spacing of the lattice. In this case the wavelengths satisfying the linear RAs condition of spatial order $\langle 0, m_2\rangle$ are

$$\lambda^{\langle 0,m_2\rangle} = \frac{n(\lambda)d_y}{|m_2|}[1 - \mathrm{sgn}(m_2)\sin(\theta)]. \tag{10}$$

Relating to the same configuration the FF wavelengths that satisfy the NL-RA condition are

$$\lambda_{\mathrm{FF}}^{\langle 0,m_2\rangle} = \frac{2d_y}{|m_2|}[n(\lambda_2) - n(\lambda_1)\mathrm{sgn}(m_2)\sin(\theta)]. \tag{11}$$

In order to experimentally examine the nonlinear interaction due to NL-RA and NL-SLR we fabricated a 50 μm × 50 μm rectangular array of gold SRRs with subwavelength x spacing of $d_x = 270$ nm and larger y spacing of $d_y = 800$ nm, which support the existence of the NL-RA, without supporting the linear RA of the FF [Figs. 1(a) and 1(b)]. Each SRR had a 180 nm base length, 180 nm arms length, 40 nm arms width, and thickness of 30 nm [Fig. 1(c)]. The sample was covered by immersion oil ($n = 1.51$), to obtain a symmetric refractive index environment, which enables the SLRs to arise stronger [19], and was placed on a rotational stage. A tunable femtosecond source (~140 fs width at 80 MHz) was used as the FF, spanning wavelengths between 1270–1580 nm (see Supplemental Material [45]). Spectral filters blocked residual SH from the OPO, and a half-wave plate and polarizer were used to control the power and polarization of the input FF. The incident beam waist was ~50 μm with an average power of ~200 mW. The emission from the sample was collected with an X20 objective lens, filtered to remove transmitted FF, and directed to an imaging spectrometer. The SH emission was verified to origin from the array and not from the substrate.

First, we examined the zero-order SH emission spectra from the array [Fig. 2(a)]. The incident light was x polarized and the collected SH light was y polarized. The SH spectra show different magnitudes of collected SH due to different physical phenomena related to $\langle 0,1\rangle$ NL-RA, $\langle 0,1\rangle$ NL-SLR, and a dark LSP mode.

The $\langle 0,1\rangle$ NL-RA, calculated according to Eq. (11), is marked by the black dots in Fig. 2(a). We see two separate regimes for wavelengths longer than ~1400 nm, distinguished by the NL-RA condition. The region on the right-hand side of the plot, where $2(k_1)_{||} + G_{0,1} > k_2$, shows about twice as bright SH compared to the region on the left-hand

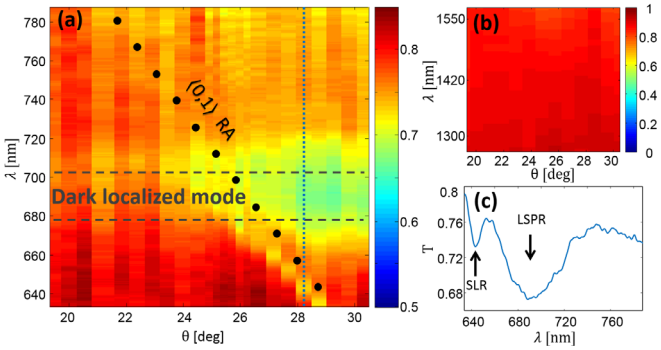

FIG. 3. Linear transmission measurements. Angle and wavelength dependent zero-order transmission of the sample at (a) the SH wavelengths range and y polarization, and (b) the FF wavelengths range and x polarization. The black dots at (a) indicate the $\langle 0,1\rangle$ RA order calculated according to Eq. (10). (c) A cross section of the transmission at (a) for angle of 28.3 degrees [blue dashed line in (a)].

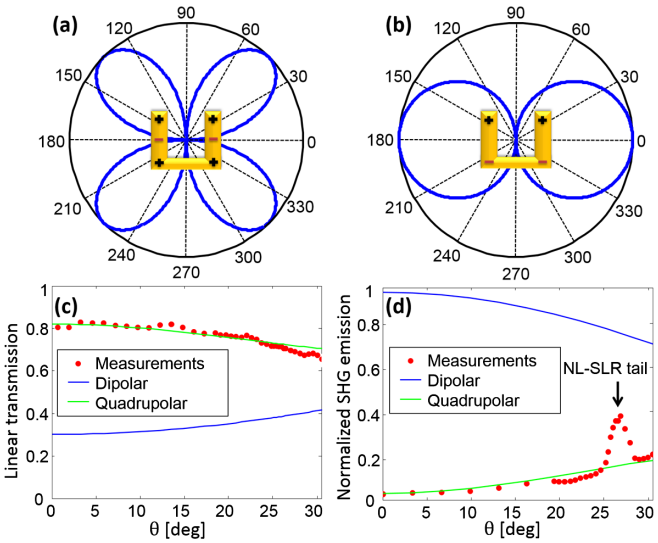

FIG. 4. Schematic charge distribution and calculated far-field radiation patterns of (a) quadrupole and (b) dipole modes, in the x-y plane. These modes exist in our nanostructures in wavelength range of 675–700 and 950–1070 nm, respectively. Angle dependent (c) transmission and (d) SH emission was calculated for quadrupole (green) and dipole (blue) modes. The measured data (red dots) agree with the behavior of a quadrupole mode for both cases. The measured data in (c) and (d) were taken by averaging the response at the wavelengths range of the quadrupole mode.

side. This difference in collected SH can be attributed to rearrangements of energy distribution between the radiating modes as the $\langle 0,1\rangle$ mode onsets or disappears, in analogy to Wood's linear observation from 1902 [15]. For wavelengths shorter than ~1350 nm strong sharp resonance behavior (~35 nm full width at half maximum) is shown at the vicinity of the NL-RA condition. We have found that this resonance behavior is the nonlinear analogue to the traditional linear SLR. It can be seen that this NL-SLR deviates from the calculated NL-RA for wavelengths approaching 1350 nm. This is due to the coupling of the nonlinear lattice mode to a nonlinear dark localized mode that exists in the wavelength range of ~1350–1400 nm. The interaction between the lattice and localized modes leads to enhancement of the collected SH compared to normal incidence that reaches a peak value of 31 around FF wavelength of 1340 nm [Fig. 2(b)].

To demonstrate that the observed phenomena are NL-RA and NL-SLR we measured also the linear interaction at FF and SH wavelength regimes. In Fig. 3(b) we show the linear angle dependent spectral transmittance at the FF wavelength regime for x-polarized light. This transmittance reveals no resonant behavior, with uniform values of ~90% all over the region of interest. The transmission spectra at the SH range [Fig. 3(a)] for y-polarized light reveals two different resonant dips in transmission. One relatively broad appearing around constant wavelengths of ~675–700 nm, and another narrow dispersive resonance [Fig. 3(c)]. It can be seen that the narrow mode exists slightly below the marked $\langle 0,1\rangle$ linear RA condition and bends when reaching the broad mode. This optical response is due to coupling between the localized and lattice resonances and existence of a hybrid SLR mode. Here we find that in contrast to most of the previous reports of SLRs [19–23,26–28], the interacting localized mode is not a bright dipole mode but a dark [24] double-quadrupole (DQ) mode on the SRR's arms [Fig. 4(a)]. This dark mode can be accessed only at oblique incidence, as seen in Fig. 3(a), in agreement with theory. We believe that the participation of the dark mode in the collective surface response is enabled by coupling of the dark mode to z-oriented dipoles in the nanoparticles as discussed in Refs. [46,47].

The dark quadrupole nature of the LSP can be deduced from the measured linear and nonlinear angle dependent behavior of the LSPR. To verify it, we compare the experimental linear and nonlinear measurements to the theoretical far-field dynamics of perfect quadrupole and dipole modes. Figures 4(a) and 4(b) illustrate schematically the charge distribution of the quadrupole and dipole modes on the arms of the SRR, respectively. Far-field radiation patterns of perfect quadrupole and dipole modes are also shown in Figs. 4(a) and 4(b), respectively. These theoretical radiation patterns were used to calculate the expected linear transmission and nonlinear emission as a function of the incidence angle. The comparison between the theoretical calculations and measurements is shown in Figs. 4(c) and 4(d) for the linear and nonlinear cases, respectively. This comparison shows a good agreement with the behavior of a dark quadrupole mode. The deviation of the fitted quadrupole curve from the measurements at the angle range of ~25–28 degrees in Fig. 4(d) is due to the fact that the mode dependent calculations do not account for the coherent coupling effect.

In addition, we performed finite element simulations (Comsol) to examine numerically the excited modes dynamics. The dielectric permittivity of gold was taken

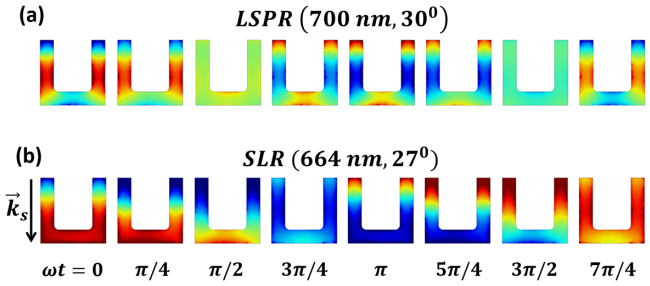

FIG. 5. Simulations of the two different resonance excitations. Surface charge distribution along the SRRs over the full optical cycle is shown in (a) at the quadrupole LSPR and in (b) at the SLR.

from Ref. [48] and for the surrounding medium we used $\epsilon = 2.3$. Periodic boundary conditions and perfectly matched layers were set along the array transverse and longitudinal directions, respectively. Figure 5(a) shows the surface charge distribution along the optical cycle on the SRR for oblique excitation at 30° and wavelength of 700 nm, which supports the excitation of a localized DQ mode. It can be seen that the evolution of the charge distribution along the optical cycle in this case shows a standing wave behavior as expected from a LSP. Figure 5(b) presents the case of excitation in the SLR conditions (angle 27°, wavelength 644 nm) which shows the transition to a propagating wave behavior with wavelength λ/n.

To conclude, we have demonstrated experimentally and theoretically the existence of NL-RA and NL-SLR in arrays of metal nanoparticles. The NL-RA condition is followed by abrupt variation in the brightness of the collinear SHG that agrees with energy rearrangement due to vanishing or onsets of the nonlinear diffraction orders. Furthermore, the NL-SLR leads to very strong and spectrally narrow enhancement of the collinear SHG. Our theoretical derivation shows that the nonlinear polarizability of the nanoparticles in the array takes a form which is similar to Miller's rule and resonantly depends on the collective nonlinear interaction. Finally, we also show that in the current case, the localized mode that hybridizes with the lattice mode to generate the NL-SLR is inherently a dark mode, which is accessible only at oblique incidence. This work reveals new dynamics of nonlinear-nonlocal interactions in arrays of metallic nanoparticles and opens the door to use such nonlocal interactions to strongly modify and enhance the effective nonlinearity of these artificial optical materials. The specific effect studied here of NL-SLR on SHG can be extended to study and enhance TWM processes and higher order nonlinear processes, which may find use in improving nanoscale multiphoton imaging, nonlinear conversion, nonlinear sensing and spectroscopy.

This publication is part of a project that has received funding from the European Research Council (ERC) under the European Union's Horizon 2020 research and innovation program (Grant Agreement No. 715362), and by the Israel Science Foundation (ISF) through Grants No. 1331/13 and No. 1433/15. S. K. acknowledges support from the Tel-Aviv University Center for Renewable Energy President Scholarship for Outstanding Ph.D. Students and the support from the Israel Ministry of Science, Technology and Space Scholarship for Ph.D. student in the field of applicative sciences.

*liormic1@mail.tau.ac.il

[1] M. W. Klein, C. Enkrich, M. Wegener, and S. Linden, Science **313**, 502 (2006).
[2] S. Linden, F. B. P. Niesler, J. Förstner, Y. Grynko, T. Meier, and M. Wegener, Phys. Rev. Lett. **109**, 015502 (2012).
[3] J. Butet, P.-F. Brevet, and O. J. F. Martin, ACS Nano **9**, 10545 (2015).
[4] N. Segal, S. Keren-Zur, N. Hendler, and T. Ellenbogen, Nat. Photonics **9**, 180 (2015).
[5] V. K. Valev, X. Zheng, C. G. Biris, A. V. Silhanek, V. Volskiy, B. De Clercq, O. A. Aktsipetrov, M. Ameloot, N. C. Panoiu, G. A. E. Vandenbosch, and V. V. Moshchalkov, Opt. Mater. Express **1**, 36 (2011).
[6] N. I. Zheludev and V. I. Emel'yanov, J. Opt. A **6**, 26 (2004).
[7] S. Campione, A. Benz, M. B. Sinclair, F. Capolino, and I. Brener, Appl. Phys. Lett. **104**, 131104 (2014).
[8] S. Kruk, M. Weismann, A. Y. Bykov, E. A. Mamonov, I. A. Kolmychek, T. Murzina, N. C. Panoiu, D. N. Neshev, and Y. S. Kivshar, ACS Photonics **2**, 1007 (2015).
[9] S. Keren-Zur, O. Avayu, L. Michaeli, and T. Ellenbogen, ACS Photonics **3**, 117 (2016).
[10] A. Rose, D. Huang, and D. R. Smith, Phys. Rev. Lett. **107**, 063902 (2011).
[11] J. B. Pendry, A. J. Holden, D. J. Robbins, and W. J. Stewart, IEEE Trans. Microwave Theory Tech. **47**, 2075 (1999).
[12] C. Ciracì, E. Poutrina, M. Scalora, and D. R. Smith, Phys. Rev. B **85**, 201403 (2012).
[13] K. O'Brien, H. Suchowski, J. Rho, A. Salandrino, B. Kante, X. Yin, and X. Zhang, Nat. Mater. **14**, 379 (2015).
[14] M. Kauranen and A. V. Zayats, Nat. Photonics **6**, 737 (2012).
[15] C. Ciracì, E. Poutrina, M. Scalora, and D. R. Smith, Phys. Rev. B **86**, 115451 (2012).
[16] S. Roke, M. Bonn, and A. V. Petukhov, Phys. Rev. B **70**, 115106 (2004).
[17] H. Husu, R. Siikanen, J. Mäkitalo, J. Lehtolahti, J. Laukkanen, M. Kuittinen, and M. Kauranen, Nano Lett. **12**, 673 (2012).
[18] L. Rayleigh, Proc. R. Soc. A **79**, 399 (1907).
[19] B. Auguié and W. L. Barnes, Phys. Rev. Lett. **101**, 143902 (2008).
[20] Y. Chu, E. Schonbrun, T. Yang, and K. B. Crozier, Appl. Phys. Lett. **93**, 181108 (2008).
[21] V. G. Kravets, F. Schedin, and A. N. Grigorenko, Phys. Rev. Lett. **101**, 087403 (2008).
[22] A. I. Väkeväinen, R. J. Moerland, H. T. Rekola, A. P. Eskelinen, J. P. Martikainen, D. H. Kim, and P. Törmä, Nano Lett. **14**, 1721 (2014).

[23] I. De Leon, M. J. Horton, S. A. Schulz, J. Upham, P. Banzer, and R. W. Boyd, Sci. Rep. **5**, 13034 (2015).
[24] A. D. Humphrey, N. Meinzer, T. A. Starkey, and W. L. Barnes, ACS Photonics **3**, 634 (2016).
[25] Z. Li, S. Butun, and K. Aydin, ACS Nano **8**, 8242 (2014).
[26] A. D. Humphrey and W. L. Barnes, Phys. Rev. B **90**, 075404 (2014).
[27] S. R. K. Rodriguez, A. Abass, B. Maes, O. T. A. Janssen, G. Vecchi, and J. Gómez Rivas, Phys. Rev. X **1**, 021019 (2011).
[28] M. Manjappa, Y. K. Srivastava, and R. Singh, Phys. Rev. B **94**, 161103 (2016).
[29] M. C. Schaafsma, A. Bhattacharya, and J. G. Rivas, ACS Photonics **3**, 1596 (2016).
[30] B. D. Thackray, V. G. Kravets, F. Schedin, G. Auton, P. A. Thomas, and A. N. Grigorenko, ACS Photonics **1**, 1116 (2014).
[31] W. Zhou, M. Dridi, J. Y. Suh, C. H. Kim, D. T. Co, M. R. Wasielewski, G. C. Schatz, and T. W. Odom, Nat. Nanotechnol. **8**, 506 (2013).
[32] N. Maccaferri, X. Inchausti, A. García-Martín, J. C. Cuevas, D. Tripathy, A. O. Adeyeye, and P. Vavassori, ACS Photonics **2**, 1769 (2015).
[33] M. Kataja, T. K. Hakala, A. Julku, M. J. Huttunen, S. van Dijken, and P. Törmä, Nat. Commun. **6**, 7072 (2015).
[34] G. Lozano, D. J. Louwers, S. Rk Rodríguez, S. Murai, O. Ta Jansen, M. A. Verschuuren, and J. Gó Mez Rivas, Light Sci. Appl. **22**, e66 (2013).
[35] G. S. Agarwal and S. S. Jha, Phys. Rev. B **26**, 482 (1982).
[36] A. C. R. Pipino, R. P. Van Duyne, and G. C. Schatz, Phys. Rev. B **53**, 4162 (1996).
[37] M. E. Inchaussandague, M. L. Gigli, K. A. O'Donnell, E. R. Méndez, R. Torre, and C. I. Valencia, J. Opt. Soc. Am. B **34**, 27 (2017).
[38] R. Czaplicki, A. Kiviniemi, J. Laukkanen, J. Lehtolahti, M. Kuittinen, and M. Kauranen, Opt. Lett. **41**, 2684 (2016).
[39] R. W. Wood, Philos. Mag. Ser. 5 **4**, 396 (1902).
[40] L. Zhao, K. L. Kelly, and G. C. Schatz, J. Phys. Chem. B **107**, 7343 (2003).
[41] F. J. García de Abajo, Rev. Mod. Phys. **79**, 1267 (2007).
[42] C. Garrett and F. Robinson, IEEE J. Quantum Electron. **2**, 328 (1966).
[43] The nonlinear polarizability-susceptibility relation is discussed in details in: R. W. Boyd, *Nonlinear Optics*, 3rd ed. (Academic Press, New York, 2008).
[44] Y. Sheng, Q. Kong, W. Wang, K. Kalinowski, and W. Krolikowski, J. Phys. B **45**, 055401 (2012).
[45] See Supplemental Material at http://link.aps.org/supplemental/10.1103/PhysRevLett.118.243904 for a detailed description of the experimental setup and measurements.
[46] M. J. Huttunen, K. Dolgaleva, P. Törmä, and R. W. Boyd, Opt. Express **24**, 28279 (2016).
[47] W. Zhou and T. W. Odom, Nat. Nanotechnol. **6**, 423 (2011).
[48] P. B. Johnson and R. W. Christy, Phys. Rev. B **6**, 4370 (1972).